

Photo-excited states in correlated band insulators

Nagamalleswararao Dasari^{1,2*} and Martin Eckstein¹

¹*University of Erlangen-Nuremberg, 91058 Erlangen, Germany and*

²*Max Planck Institute for the Structure and Dynamics of Matter, 22761 Hamburg, Germany.*

We study the photo-excitation dynamics of correlated band insulators, using non-equilibrium dynamical mean-field theory for the ionic Hubbard model. We find two distinct behaviors, depending on the ratio of the on-site interaction U and the bare band gap Δ . For small interactions, the relaxation is characterized by intra-band carrier scattering in relatively rigid bands, leading to a non-thermal intermediate state with separate thermal distributions of electrons and holes. This behavior can be viewed as typical for a band insulator with weak interactions. For larger interaction, on the other hand, we observe a strong modification of the electronic spectrum and a filling-in of the gap after photo-excitation, along with a rapid thermalization of the system. The two behaviors therefore provide a dynamical distinction of a correlated band insulator and a band-insulator, which can differ even when the spectra of the two systems are similar in equilibrium. The crossover happens when the interaction U is comparable to Δ .

I. INTRODUCTION

The possibility to switch quantum states through ultrafast non-thermal pathways has made non-equilibrium studies of quantum many-body systems attractive to the condensed matter community.¹ Using laser photo-excitation or external electric fields one can induce transient states on short time-scales, and in some cases even long-lived hidden quantum states, with electronic properties which are entirely different from equilibrium.²⁻⁵

A rich variety of novel phases in non-equilibrium can be expected for strongly correlated systems. Electronic correlations are predominantly studied in systems which are metallic in the non-interacting limit. In these systems, correlations result in phenomena like the Mott transition, high-temperature superconductivity, and non-Fermi liquid behavior. In band insulators, in contrast, one may naively expect that the existence of the band gap and the absence of low energy quasi-particles reduces the importance of electronic correlations. However, this turns out to be not true. The role of electronic correlations in band insulators has been studied in various models, including the ionic Hubbard model,⁶⁻¹⁷ a two orbital Hubbard model with crystal-field splitting,¹⁸ a two sub-lattice model with inter-orbital hybridization^{19,20} and a bilayer model with two identical Hubbard planes.²¹⁻²⁵ In general, at weak-coupling the competition between the local Coulomb interaction and the non-interacting band gap results in a correlated band insulator with a renormalized gap. Further increasing the interaction strength can even close the gap, and lead to an interaction-driven metal or bond-ordered state in the strong coupling limit.^{10,11,19} The renormalized band gaps and the difference in charge and spin gaps distinguishes correlated band insulators from non-interacting band insulators.^{6,7,19} Correlated band insulators provide a paradigm example for systems with competing ground state interactions, and hence are good candidates to explore hidden quantum states through non-thermal pathways.

In a band insulator, photo-excitation will promptly

lead to a partial occupation of the conduction band. At weak coupling, one may expect the dynamics of such systems to be similar to semiconductors: Interactions provide a mechanism for electron-electron scattering, while the bands which are almost rigid apart from some photo-induced screening of the gap which is largely included in a Hartree shift of the bands. This leads to a state in which electrons and holes are separately thermalized in the conduction and valence band. On longer timescales, the system would establish a common temperature and chemical potential, and the energy is passed to the lattice. Such processes in semiconductors are well described using quantum Boltzmann equations.²⁶ In this paper, we explore how this picture is modified at larger interaction, and whether there is a distinct dynamical behavior of band insulators and correlated band insulators. How is the gap renormalized or even filled due to local correlations after photo-excitations? What is the role of these correlations on the thermalization process: Does the filling in of the gap lead to a speed-up of thermalization, and is there room for non-thermal metallic states?

The theoretical study of such systems out of equilibrium is challenging. Kinetic equations cannot describe a change of the electronic structure due to local correlations. In the past few years, non-equilibrium dynamical mean-field theory (DMFT) has been widely applied to study the photo-excitation and quench dynamics of correlated electronic systems.²⁷ In this work, we study the dynamics of correlated band insulators by means of non-equilibrium DMFT, using iterative perturbation theory (IPT) as an impurity solver. We find a crossover between two different behaviors when the local Coulomb interaction becomes comparable to the non-interacting band gap. The typical behavior of a band insulator with two separate sub-systems of thermalized holes and electrons persists only for the smaller interaction.

The paper is organized as follows. In section II, we present the model and method used to study the photo-excitation of correlated band insulators, and briefly discuss the equilibrium properties of the model. In section III we present the numerical results, and Sec. IV contains

an analysis and discussion.

II. MODEL AND METHOD

A. Ionic Hubbard model and DMFT

Correlated band insulators are well described by the ionic Hubbard model (IHM) on a bipartite lattice with two sub-lattices A and B . The Hamiltonian is given by

$$\mathcal{H} = -J(t) \sum_{\langle i,j \rangle} [c_i^\dagger c_j + H.c.] + \Delta \sum_{i \in A} n_i - \Delta \sum_{i \in B} n_i + U \sum_i n_{i\uparrow} n_{i\downarrow} - \mu \sum_i n_i, \quad (1)$$

where J is the nearest neighbour hopping amplitude, and U is the on-site Coulomb interaction. The staggered ionic potential Δ is the origin of the non-interacting band gap. We choose the chemical potential μ such that total filling of the system is fixed at half-filling ($n_A + n_B = 1$). At half-filling, the above Hamiltonian describes a band insulator and a Mott insulator in the limits ($U = 0, \Delta \neq 0$) and ($U = \infty, \Delta = 0$), respectively. Nontrivial states arise when both Δ and U are nonzero and finite.

To study the photo-excitation dynamics of correlated band insulators we employ the non-equilibrium DMFT formalism,²⁷ which is exact in the limit of infinite-coordination number (Z) with hopping $J(t) = J^*/\sqrt{Z}$. We choose a non-interacting dispersion of bands on a bipartite lattice, with a semi-elliptical density of states $\rho(\epsilon) = \frac{1}{\pi J^*} \sqrt{4J^{*2} - \epsilon^2}$. We set the half bandwidth $2J^* = 1$ as energy unit, and the unit of time is $\frac{\hbar}{2J^*}$. The DMFT formalism makes a local approximation for the self-energy, i.e., $\Sigma_{ij}(t, t') \approx \Sigma_{ii}(t, t')$ which allows to map the lattice problem Eq. (1) to an effective quantum impurity problem with a self-consistently determined bath $\Gamma(t, t')$. The impurity action for sub-lattice $\alpha \in \{A, B\}$ is given by

$$S_\alpha = \int_C dt H_{loc}^\alpha(t) + \sum_\sigma \int_C dt dt' c_{\sigma\alpha}^\dagger(t) \Gamma_\alpha(t, t') c_{\sigma\alpha}(t). \quad (2)$$

Here C is the Keldysh time contour (for an introduction into the Keldysh formalism, see, e.g., Ref. 27), and

$$H_{loc}^\alpha = U n_{\uparrow}^\alpha n_{\downarrow}^\alpha + [\Delta_\alpha - \mu](n_{\uparrow}^\alpha + n_{\downarrow}^\alpha) \quad (3)$$

is the local Hamiltonian on the impurity, with $\Delta_A = \Delta$ and $\Delta_B = -\Delta$. The semi-elliptical density of states yields a closed form expression for the self-consistency relation, which is given by $\Gamma_\alpha(t, t') = J^*(t) G_{\bar{\alpha}}(t, t') J^*(t')$, where $G_\alpha(t, t') = -i \langle T_C c_\alpha(t) c_\alpha^\dagger(t') \rangle_{S_\alpha}$ is the local Green's function defined on Keldysh contour ($\bar{\alpha} = B$ for $\alpha = A$ and vice versa). For a given sub-lattice hybridization Γ_α , the local Green's functions G_α can be determined from the Dyson equation,

$$[i\partial_t + \mu + \Delta_\alpha - \Sigma_\alpha - \Gamma_\alpha] G_\alpha = 1, \quad (4)$$

where Σ_α is local self-energy which is calculated from the effective impurity problem. We use the real-time iterative perturbation theory (IPT) as an impurity solver to calculate the local self-energy. The diagrammatic expression for the IPT ansatz is given by

$$\Sigma_\alpha(t, t') = \sqrt{A^\alpha(t) A^\alpha(t')} U(t) U(t') \times \mathcal{G}_\alpha^H(t, t') \mathcal{G}_\alpha^H(t, t') \mathcal{G}_\alpha^H(t', t), \quad (5)$$

where \mathcal{G}_α^H is the Hartree-corrected bath propagator, which is given by the Dyson equation

$$[i\partial_t + \mu - \Delta_\alpha - \Sigma_H^\alpha - \Gamma_\alpha] \mathcal{G}_\alpha^H = 1, \quad (6)$$

with the Hartree self-energy $\Sigma_H^\alpha(t, t') = U n^\alpha(t) \delta_c(t, t')$. Following Ref. 10, the factors A^α in Eq. (5) are chosen such that in equilibrium the ansatz is exact in the weak-coupling limit ($U/t \ll 1$) and it has the exact short time behavior for all values of U/t , which imposes various exact sum rules. The corresponding expression for $A^\alpha(t)$ is $n_\alpha(t)(1 - n_\alpha(t))/n_\alpha^0(t)(1 - n_\alpha^0(t))$ where $n_\alpha^0(t)$ is the impurity occupancy, which is calculated from \mathcal{G}_α^H . Writing the A -factor in the symmetrized form $\sqrt{A^\alpha(t) A^\alpha(t')}$ guaranties that the self-energy Eq. (5) is hermitian, while the expression reduces to the conventional form $\sqrt{A^\alpha(t) A^\alpha(t')} = A_\alpha$ at equilibrium, when A_α is time independent.

Non-equilibrium DMFT measures the local Green's function for each sub-lattice. The sub-lattice occupancy is obtained from the equal-time lesser component of the Green's function, $m(t) = n_A(t) - n_B(t) = -iG_A^<(t, t) + iG_B^<(t, t)$. To find the effective temperature of the photo-excited system we need to calculate the total energy of the system, which is the sum of kinetic energy, interaction energy and lattice potential energy. The kinetic energy of photo-excited system is given by the equal-time contour convolution of the hybridization function with the local Green's function, $E_{kin} = -i \sum_\alpha [\Gamma_\alpha * G_\alpha]^<(t, t)$, and the interaction energy is the equal-time contour convolution of the local self-energy with the local Green's function, $E_{int} = i \sum_\alpha [\Sigma_\alpha * G_\alpha]^<(t, t)$.²⁷ The lattice potential energy is $E_\Delta(t) = \Delta(n_A(t) - n_B(t))$. The double occupancy $d_\alpha(t) = \langle n_{\uparrow}^\alpha n_{\downarrow}^\alpha \rangle$ is obtained from the interaction energy.

One of the issues with IPT is the non-conserving nature of the self-energy in the sense of Baym-Kadanoff. A violation of the energy conservation can be identified when there is a drift of the total energy with time even though the Hamiltonian is time independent. In previous non-equilibrium DMFT calculations for interaction quenches in a single-band Hubbard model it was found that IPT conserves the total energy very accurately up to all accessible simulation times in the weak-to-intermediate coupling regime, while with increasing U there is a relatively sharp crossover after which only the short time dynamics is correctly captured.²⁸ In this work we focus on relatively weak coupling, and we have confirmed that an unphysical short-time increase of the energy as observed in Ref. 28 does not occur.

B. Equilibrium DMFT study of the IHM

A first understanding of the equilibrium states of the IHM can be obtained from the atomic limit $J/U=0$, at total filling equal to 1. In this trivially soluble limit, the ground state for $U < 2\Delta$ has two electrons on sublattice B and zero on sublattice A , resulting a band insulator with a band gap $\Delta - U/2$. In the opposite limit ($U > 2\Delta$) each sublattice is occupied by one electron, and we get a Mott insulator with a gap U . In the atomic limit, the system is gapless at $U=2\Delta$. An interesting question therefore is whether local correlations broaden this metallic point into a metallic phase when J is non-zero.

Equilibrium studies of the IHM at zero temperature using DMFT with an IPT impurity solver, find that electronic correlations strongly renormalize the non-interacting band-gap for small values of U . The gap in the spectral function vanishes at a critical interaction U_c , and the system is metallic for a finite range of interactions.^{10,12} As we further increase $U > U_c$, the system becomes Mott insulating, i.e., the gap in the spectral function opens again and increases with U . The crossover from a correlated band insulator to a metal has been observed experimentally in photoemission spectra of $\text{SrRu}_{1-x}\text{Ti}_x\text{O}_3$.²⁹

IPT studies of the IHM find the metallic phase only up to intermediate values of Δ , while for large values of the ionic potential there is a direct transition from a band insulator to a Mott insulator.^{10,12} A recent study of the IHM at finite temperature using a continuous-time quantum Monte Carlo (CTQMC) impurity solver has obtained a phase diagram similar to IPT for intermediate values of Δ , but in contrast to IPT the intermediate metallic phase persists to even larger values of Δ .¹⁵ An open issue is the nature intermediate metallic phase.¹² 2D-cluster extensions of DMFT find a bond-ordered phase as an intermediate metallic phase,¹¹ while single-site DMFT using CTQMC suggests that the intermediate metallic phase is a Fermi-liquid.¹⁵

C. Photo-doping

Photo-doping changes the electron-hole concentration by irradiating light on the sample. Experimentally, laser photo-excitation not only changes the carrier concentration of the bands at the Fermi-level, but it can also excite electrons from bands far below the Fermi-level into the conduction band, and electrons from the valence band to other bands far above the Fermi-level. In our work, we employ this setup to induce photo-excited state. To mimic such an experimental situation theoretically, one can couple two additional wide-band particle reservoirs to the system. One reservoir is entirely filled and will therefore inject particles into the empty states of the system, while the other one is empty and can take out electrons from occupied states. The additional fermionic baths are

non-interacting and can be integrated out exactly. The resulting DMFT action is the same as Eq. (2), but the hybridization function is modified to

$$\Gamma'_\alpha(t, t') = \Gamma_\alpha(t, t') + \Gamma^{\text{filled}}(t, t') + \Gamma^{\text{empty}}(t, t'). \quad (7)$$

Here the first term corresponds to the self-consistent hybridization of the ionic Hubbard model, and the last two terms correspond to the hybridization of the filled and empty reservoirs. The latter are given by

$$\Gamma^{\text{filled/empty}}(t, t') = h(t)G^{\text{filled/empty}}(t, t')h(t'), \quad (8)$$

where $G^{\text{filled/empty}}$ is the Green's function of the reservoir, and $h(t)$ is the time-profile of the coupling between the IHM and the reservoirs, for which we take the form

$$h(t) = h_0 \sin(\pi t/t_{\text{pulse}}), \quad (9)$$

for $t \leq t_{\text{pulse}}$ and $h(t) = 0$ for $t > t_{\text{pulse}}$. Throughout this work we fix $t_{\text{pulse}}=3.0$, and h_0 is chosen to control the excitation density. The density of states corresponding to $G^{\text{filled/empty}}(t, t')$ is a Lorentzian of width $8J^*$.

III. RESULTS

We start the analysis of relaxation after photo-excitation with an investigation of the time-dependent double occupancy and the sublattice occupation (Sec. III A and III B), and then proceed to analyze spectral functions and the occupation function (Sec. III C). To know whether the photo-excited system thermalizes after the pulse, we need to find the effective temperature T_{eff} of the time-evolved state.³⁰ For this purpose, we determine a thermal equilibrium state which has the same energy as the time-evolved state. The corresponding temperature of the equilibrium state then defines T_{eff} . (In practice, we choose the excitation density in order to fix a given effective temperature, $T_{\text{eff}} = 1$ or $T_{\text{eff}} = 0.3$.) With this we can compare time-dependent expectation values of various observables $O(t)$ to corresponding expectation values $O_{th} \equiv O(T_{\text{eff}}) = \text{Tr}[\exp^{-H/T_{\text{eff}}} O]/Z$. Throughout the paper we fix a low initial temperature T by $\beta = 1/T = 32$.

A. Thermalization of the metal ($\Delta = 0$)

When the ionic potential is zero, the IHM reduces to a simple one-band Hubbard model with intra-orbital interaction U , which is metallic at small values of U . In order to later contrast the results to the correlated band insulator, we first investigate the thermalization of this metallic phase within our formalism. In Fig. 1(a), we plot the time-dependent double occupancy $d(t) = \langle n_\uparrow n_\downarrow \rangle$ of the photo-excited system for different values of U . We fit the time-dependent double occupancy to a single exponential function $d(t) = d_{t=\infty} + b \exp(-t/\tau_d)$ and extract

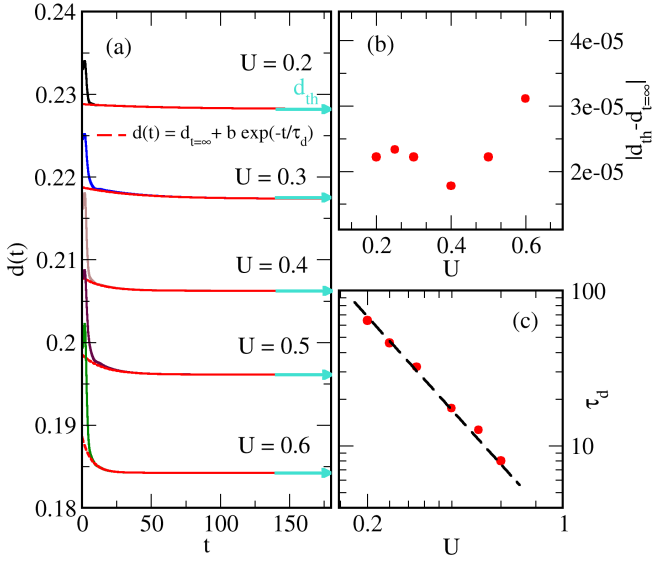


FIG. 1. (a) Double occupancy of the photo-excited system for different values of U values. The excitation density is chosen such that $T_{\text{eff}} = 1$. Solid curves show the numerical data, and red dashed lines show exponential fits. Small arrows indicate the double occupancy in thermal equilibrium. (b) Difference of the double occupancy in equilibrium at temperature $T = T_{\text{eff}}$ and in the photo-excited system. (c) Relaxation time of the double occupancy for different values of U . The dashed curve is a fit to the relaxation times with the relation $\frac{a}{U^2}$.

the extrapolated value $d_{t=\infty}$ of $d(t)$ in the long time limit and the corresponding relaxation times τ_d . The thermal values d_{th} of the double occupancy, obtained from equilibrium simulations at the corresponding effective temperature are shown by arrows in Fig. 1(a). The difference $|d_{th} - d_{t=\infty}|$ is plotted in Fig. 1(b). One can see that the time-dependent double occupancy approaches d_{th} in the long-time limit for all values of U within our numerical accuracy, which implies thermalization of the weakly-correlated metal. The relaxation times τ_d are plotted in Fig. 1(c). The thermalization times can be fit well with a power law $\tau_d \sim 1/U^2$. This behavior is consistent with a quasi-particle picture: In the different calculations we have chosen the excitation such that the effective temperature is fixed to $T_{\text{eff}} = 1$, so that the phase space for scattering is fixed, and the scattering rate is given by the scattering matrix element, which is proportional to U^2 .

B. Correlated band insulator: relaxation of the double occupancy and the sub-lattice occupation

To study the relaxation dynamics of the correlated band insulator, we analyze the relaxation dynamics of the time-dependent double occupancy $d^A(t)$ (measured at the A sub-lattice without loss of generality). Analogous to the previous paragraph, we extract the value of the double occupancy at infinite time ($d_{t=\infty}^A$) and the

relaxation time (τ_d^A) from an exponential fit $d^A(t) = d_{t=\infty}^A + b \exp(-t/\tau_d^A)$. In the upper panel of Fig. 2, we plot the difference of d_{th}^A to the time evolved value $d_{t=\infty}^A$ for different values of the ionic potential. In contrast to the metal, $|d_{th}^A - d_{t=\infty}^A|$ approaches zero only when $U/\Delta \gtrsim 1$. This implies that for smaller interactions, the observed relaxation on the timescale of our simulation is towards a non-thermal state, while the behavior at large interactions is consistent with thermalization. The crossover from non-thermal to thermal behavior occurs roughly when U is of the order of Δ , but it also depends on the excitation density (i.e., the effective temperature of the final state). In the lower panel of Fig. 2, we plot the relaxation times τ_d^A obtained from the exponential fits. In the regime where the system thermalizes ($U/\Delta \gtrsim 1$), the relaxation times decrease with U , like in the metal. In the opposite limit, the relaxation depends on U in a non-monotonous way, and reaches a maximum value around $U/\Delta \approx 0.6$.

The sub-lattice occupancy $m(t) = n_A(t) - n_B(t)$, exhibits a similar behavior as observed for the double occupancy. For this purpose, we again analyze $m(t)$ by means of an exponential fit, $m(t) = m_{t=\infty} + b \exp(-t/\tau_m)$. The upper panel of Fig. 3 shows the difference of m_{th} and $m_{t=\infty}$ for the same parameters as in Fig. 2. Similar to the double occupancy, the sub-lattice occupation $m(t)$ displays a crossover from non-thermal to thermal behavior when U is comparable to the ionic potential, with the same trend in the relaxation times τ_m (lower panel of Fig. 3).

C. Relaxation of the spectral function

The observed crossover from non-thermal to thermal behavior can be further analyzed by looking at the spectral functions and the occupation function. The analysis of the spectral function furthermore allows to access the possible transient metallicity of the photo-doped state. To identify any such metallic states we calculate the single particle spectral function $A^R(\omega, t)$ and the occupied density of states $A^<(\omega, t)$ from a Fourier transform,

$$A^\gamma(t, \omega) = \mp \frac{1}{\pi} \text{Im} \int_0^t ds e^{i\omega s} G^\gamma(t, t-s). \quad (10)$$

Here the upper and lower sign corresponds to the spectral function ($\gamma=R$) and the occupied density of states ($\gamma=<$), respectively. The occupied density of states are closely related to the intensity in time-dependent photoemission spectroscopy.³¹ Note that in non-equilibrium, we can define the Fourier transform of a function $G(t, t')$ with respect to time-difference in forward ($t' > t$), backward ($t' < t$), or symmetric fashion. Since we analyze spectra at the largest time when the system is almost in a steady state, the differences are minor, and we have chosen the backward form (10) unless stated otherwise.

In the left panels of Fig. 4(a) and (b), we compare the time-dependent spectral function in the photo-doped

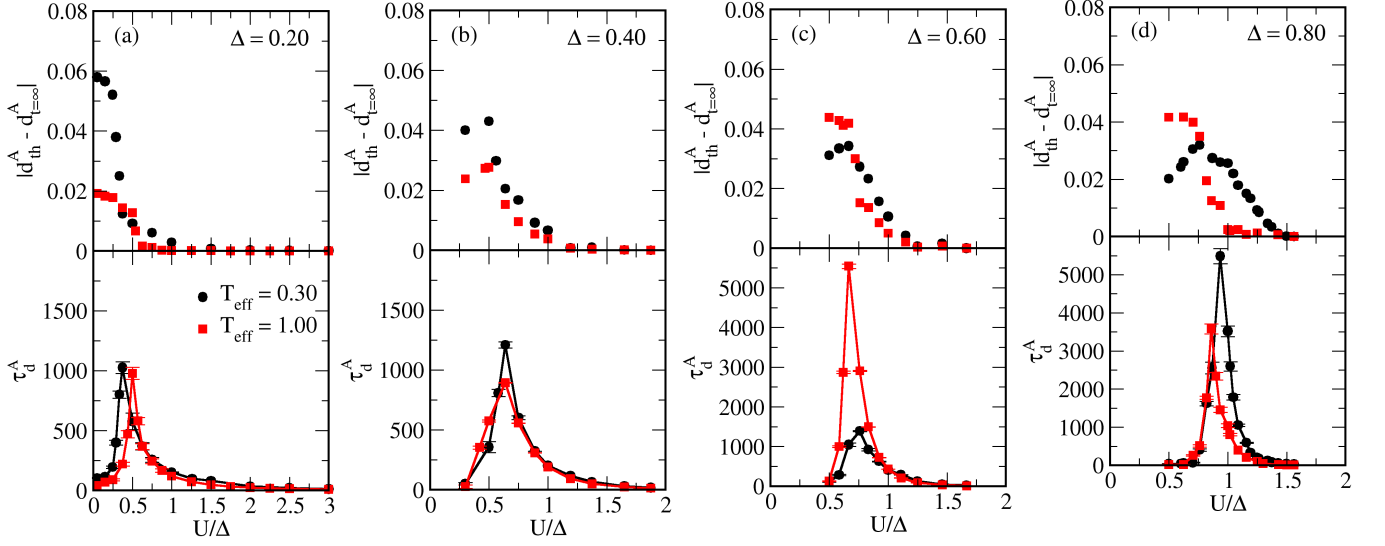


FIG. 2. Upper panel: Difference of the double occupancy in thermal equilibrium at temperature $T = T_{eff}$ and in the time-evolved state, for different values of the ionic potential (a) $\Delta = 0.2$ (b) $\Delta = 0.4$ (c) $\Delta = 0.6$ (d) $\Delta = 0.8$. The excitation density is chosen such that $T_{eff} = 0.3$ (black circles) or $T_{eff} = 1.0$ (red squares). Lower panel: Relaxation times of the double-occupancy.

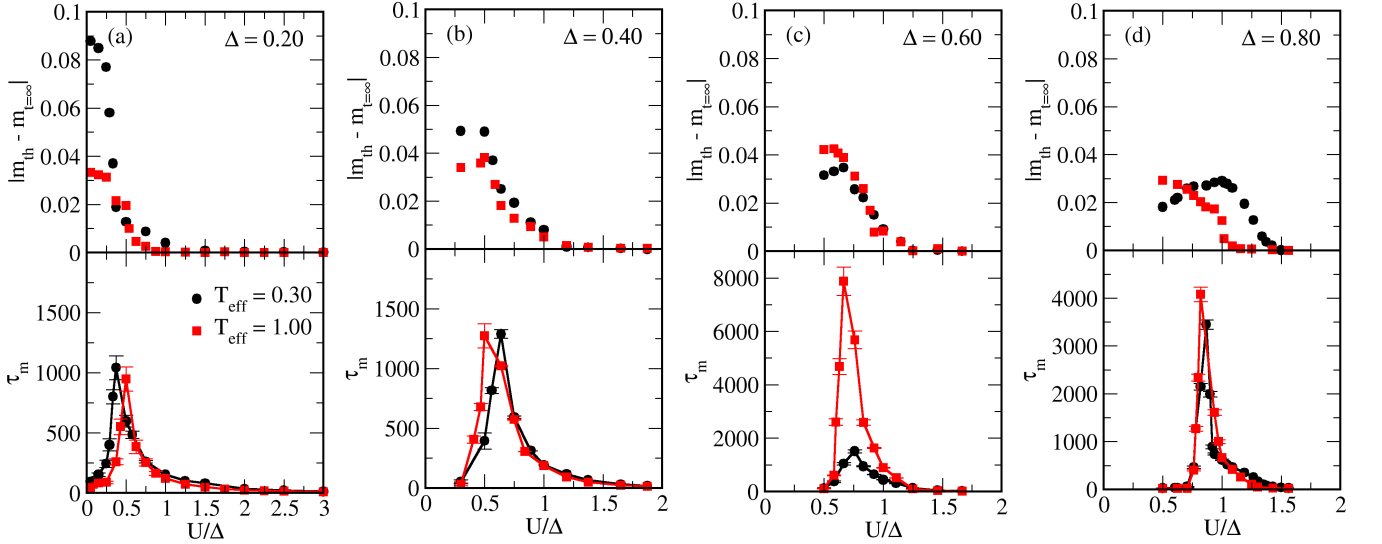


FIG. 3. Upper panel: Difference of the sub-lattice occupancy in thermal equilibrium (m_{th}) at temperature $T = T_{eff}$ and in the time-evolved state ($m_{t=\infty}$), for different values of the ionic potential (a) $\Delta = 0.2$ (b) $\Delta = 0.4$ (c) $\Delta = 0.6$ (d) $\Delta = 0.8$. The excitation density is chosen such that $T_{eff} = 0.3$ (black circles) or $T_{eff} = 1.0$ (red squares). Lower panel: Relaxation times of the sub-lattice occupancy.

state (green solid lines) and in the equilibrium state (magenta dashed lines) for $\Delta = 0.4$ [Fig. 4(a)], $\Delta = 0.6$ [Fig. 4(b)], and different values of U . The corresponding occupation functions are shown in the right panels. In the thermal spectra, we find a well-defined gap at small values of U . The gap is robust even though the temperature is larger than U and Δ , i.e., the main effect of the temperature is the occupation of states in the upper band, as seen from the occupied density of states in the right panel. Increasing values of U lead to a renormalization of the gap, and a broadening of the square-root

singularity at the gap edge. When U is of the order of the ionic potential, the gap in the spectral function starts to fill, until it is completely melted for large U . Hubbard bands would only emerge at larger values of U . Similar as for the double occupancy, a significant difference between thermal and photo-excited systems in $A^<(\omega)$ is apparent only for $U \lesssim \Delta$, confirming the non-thermal nature of the photo-excited state in this regime. Interestingly, the difference between thermal and photo-excited states is almost invisible for the retarded spectral function on the energy scale plotted in the left panel of Fig. 4(a) and (b),

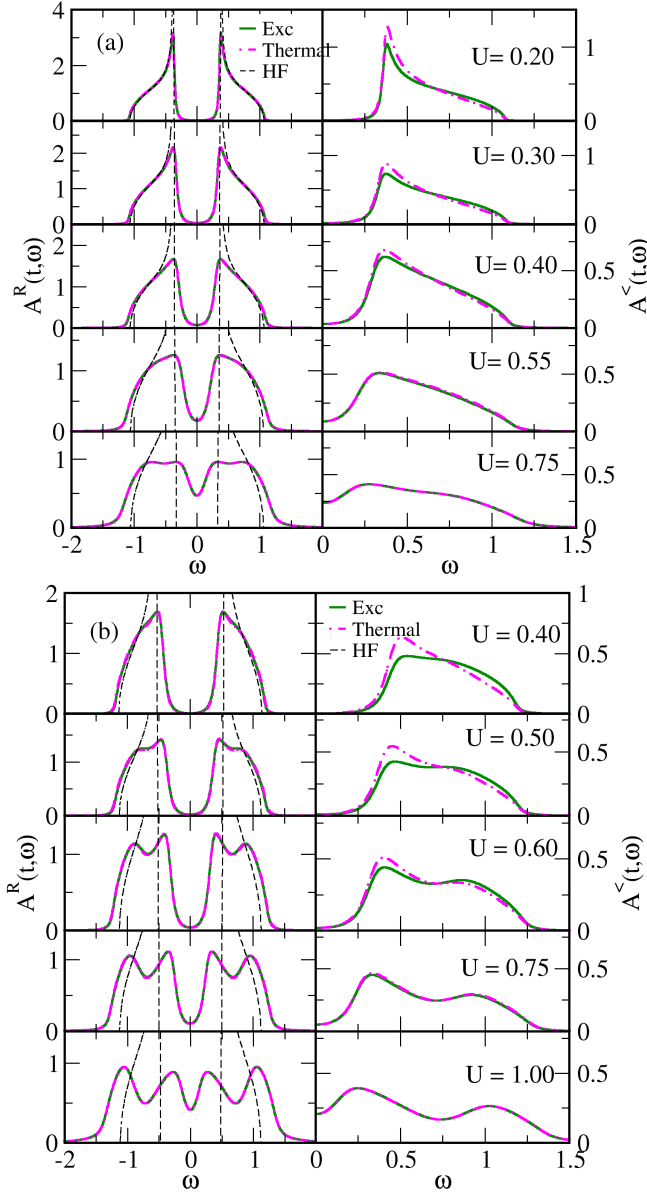


FIG. 4. (a) Left panel: Spectral function $A^R(t = 180, \omega)$ for different values of U and $\Delta = 0.4$. (a) Right panel: The corresponding occupied density of states $A^<(t = 180, \omega)$ above the Fermi-level. The black dashed lines indicate the Hartree-Fock spectral function (see text) (b) Same as (a) but for $\Delta = 0.6$. The excitation density is chosen such that $T_{\text{eff}} = 1$.

which will be discussed below (Sec. IV A).

The thermalization can be further verified by checking whether the electronic Green's functions satisfy the fluctuation-dissipation theorem (FDT). In equilibrium, the FDT implies a ratio $A^<(\omega)/A^>(\omega) = e^{-\beta(\omega-\mu)}$ between the occupied density of states $A^<(\omega) = -iG^<(\omega)$ and the unoccupied density of states $A^>(\omega) = iG^>(\omega)$, or equivalently a ratio $A^<(\omega)/A^R(\omega) = 1/(1 + e^{\beta(\omega-\mu)})$ between the occupied density of states and the spectral function. To test whether the photo-doped state is in a quasi-equilibrium state, we therefore calculate the partial

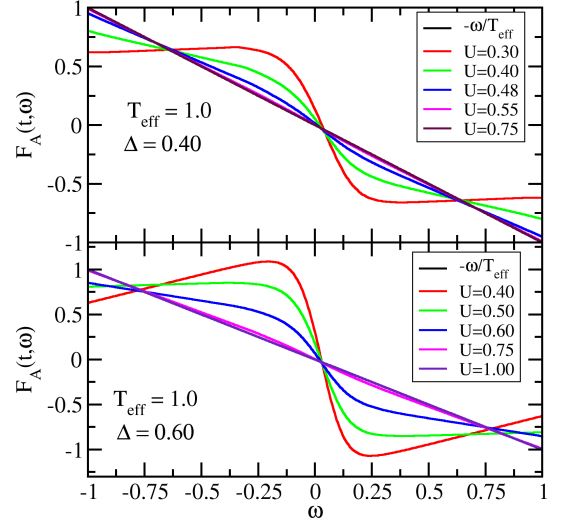


FIG. 5. Electronic distribution functions $F_A(t = 180, \omega)$ [Eq. (11)] for different values of U and ionic potential $\Delta = 0.4$ (upper panel) and $\Delta = 0.6$ (lower panel).

Fourier transform $A^{<,>}(t, \omega)$ as in Eq. (10), and evaluate the quantity

$$F_A(t, \omega) = \log \left(\frac{A^<(t, \omega)}{A^>(t, \omega)} \right), \quad (11)$$

which reduces to $-(\omega - \mu)/T_{\text{eff}}$ in a quasi-equilibrium state. In Fig. 5, we plot $F_A(t, \omega)$ for a given Δ and different values of U . The FDT is satisfied when the local Coulomb interaction is greater than the ionic potential $U > \Delta$, which confirms that the photo-excited electrons have reached an equilibrium state. Furthermore, in this limit the effective temperature obtained from the FDT analysis accurately matches the value $T_{\text{eff}} = 1$ obtained from the total energy.

For $U \lesssim \Delta$, however, the electronic distribution functions are highly non-thermal. Nevertheless, $F_A(t, \omega)$ takes a linear form $(a + b\omega)$ in the spectral region outside the gap ($|\omega| \gtrsim 0.3$). This can be interpreted in the form of two distinct Fermi functions with different chemical potentials in the upper and lower band, respectively. This signals thermalization of electrons and holes as two separate sub-systems due to intra-band scattering. The effective temperatures of such photo-doped states are very large (the distribution functions are almost flat) or even negative, corresponding to a population inversion. In photo-doped Mott insulators with long-range Coulomb interactions, self-sustained population inversions have been found in the photo-doped state.³² In the present case, however, the effective temperature is mainly governed by the carrier distribution during the photo-doping process.

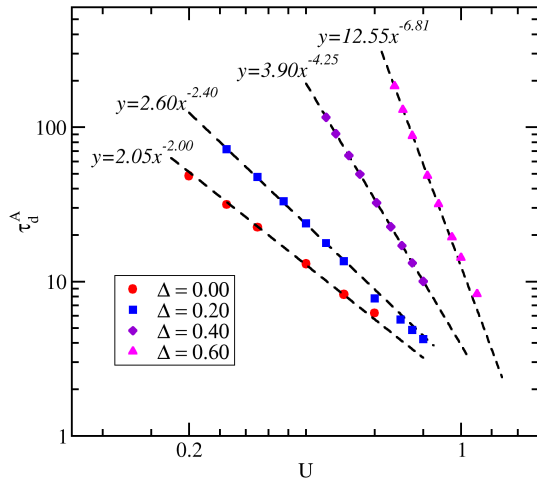


FIG. 6. Relaxation times of the double occupancy for different values of Δ and $U > \Delta$. The dashed curves indicate power law fits.

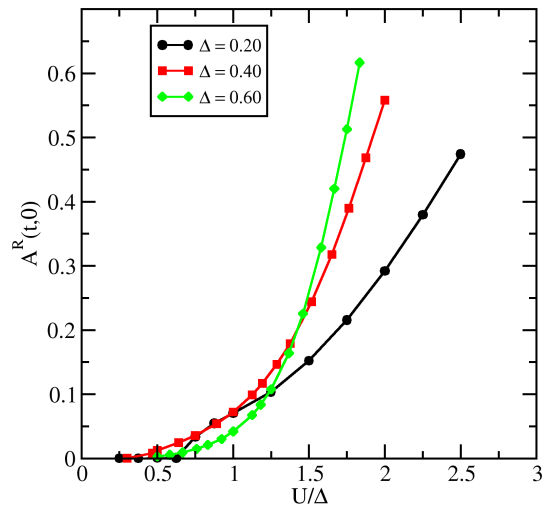


FIG. 7. The value of the retarded spectral function at $\omega=0$ for large time $t=180$ in the photo-excited state (excitation density such that $T_{\text{eff}} = 1$).

IV. DISCUSSION

A. Crossover from a band-insulator to a correlated band insulator

Summarizing the previous section, one can say that the behavior of the system for $U \lesssim \Delta$ is well described by the expectation for a band insulator, which is characterized by the following features:

(i) At temperatures of interest for photo-excitation, the (retarded) spectral function is relatively rigid. Up to a trivial Hartree shift, which depends only on the thermal or photo-induced sub-lattice occupation, it is barely influenced by increasing the temperature or photo-doping. This is seen by a comparison of thermal, photo-excited,

and Hartree spectra in Fig. 4. The fact that the spectra only weakly depend on the occupation also explains why the difference between thermal and photo-excited spectra is small in this regime.

(ii) The main relaxation mechanism is intra-band relaxation, i.e., scattering between electrons and holes. Only few scattering processes lead to a redistribution of carriers across the gap. This is consistent with the establishment of separate thermalized distributions in the region of the upper and lower band, as shown in Fig. 5. The absence of a global thermal state with a common chemical potential also explains the non-thermal behavior observed in the double occupancy and the sub-lattice occupation, which are quantities that involve both valence and conduction band states and thus can indicate global thermalization.

Above the crossover $U \approx \Delta$, the behavior of the system changes drastically. In this regime, photo-excitation leads to a partial filling-in or closing of the gap, and rapid thermalization. As the system thermalizes in the correlated band insulating regime, it is interesting to compare the thermalization times from Figs. 2 and 3 with those observed in the metal (Fig. 1). In Fig. 6, we plot the thermalization times of the double occupancy for different values of the ionic potential and $U > \Delta$. We find that the decrease of the thermalization time with U in the correlated band insulator is faster compared to the metal. The thermalization timescale is rather well described with a behavior $1/U^n$ with $n > 2$ ($n = 2$ for the metal), and the value of n increases rapidly with the ionic potential. The large value of n signifies that the thermalization dynamics of correlated band insulators is different from metals.

In Fig. 7 we show the spectrum $A^R(0)$ at the Fermi-level as a function of U/Δ for different values of Δ . A nonzero density of states at the Fermi-level gives a finite phase-space volume for photo-doped carriers to exchange the energy and thus can lead to fast thermalization of the photo-excited system. For $U \gtrsim \Delta$, the weight at the Fermi-level increases strongly with U/Δ . The larger exponent n in Fig. 6 is therefore a consequence of the combined increase of the interaction U and the spectral weight.

B. Role of Impact ionization

Recently it was shown that impact ionization processes can take an important role in the thermalization and relaxation of photo-excited Mott insulators.³³ Impact ionization occurs if the kinetic energy of charge carriers is larger than the size of the Mott gap, so that it is energetically allowed to create an additional doublon-hole pair via two-particle scattering. Impact ionization can be identified by the following characteristic signatures in the occupation function: (i) An impact ionization process decreases the occupied density of states at high energies, and increases it at energies which are lower by at least

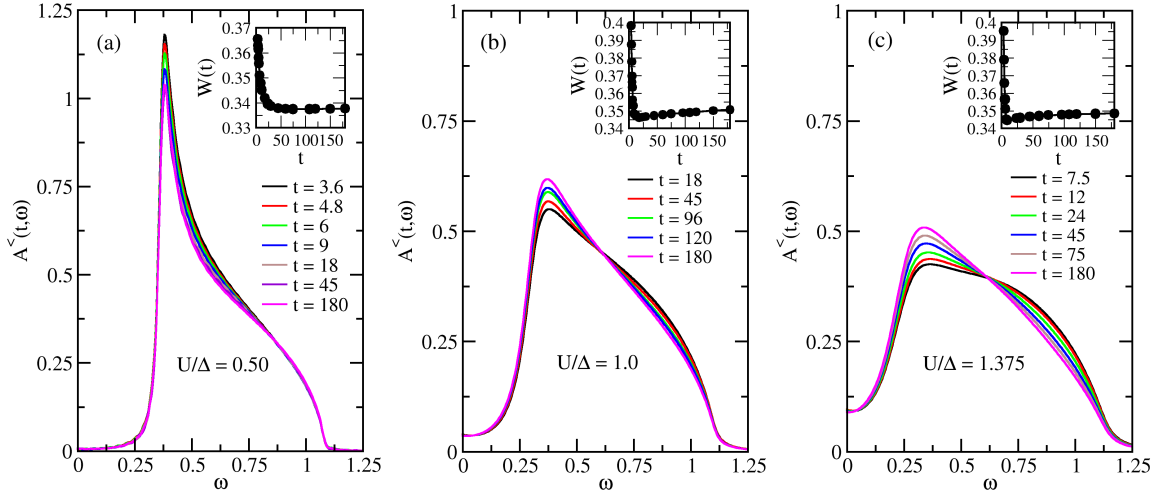


FIG. 8. Occupied density of states above the Fermi-level at different times for $\Delta=0.4$ and $T_{\text{eff}}=1.0$. Insets: Integrated weight of the occupied density of states, $W(t)=\int_0^\infty A^<(t, \omega) d\omega$ above the Fermi-level.

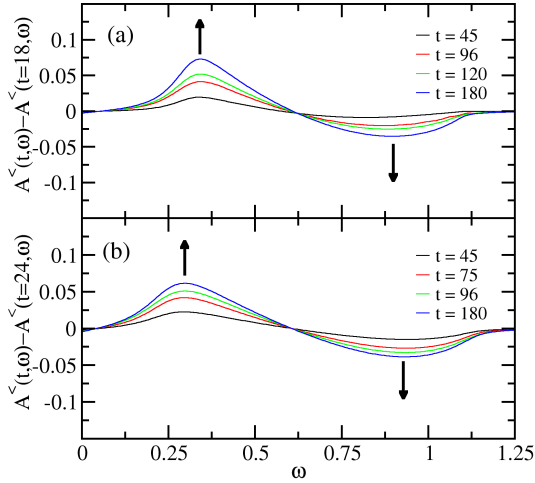


FIG. 9. Time dependent change of the occupied density of states for excitation density corresponding to $T_{\text{eff}}=1.0$, $\Delta=0.4$, and (a) $U/\Delta = 1.0$ (b) $U/\Delta = 1.375$. The up (down) arrows indicates frequencies at which rapid increase (decrease) most strongly during the relaxation.

the size of the gap. (ii) Impact ionization processes increase the density mobile carriers, and hence increase of integrated spectral weight above the gap.

To see whether impact ionization processes are important in the thermalization of correlated band insulators, we plot the time-dependent lesser spectral function for three different ratios of $U/\Delta=0.5, 1.0$ and 1.375 (see Fig. 8). For $U/\Delta = 0.5$ [Fig. 8(a)], the photo-excited system is not yet thermalized and there is a well-defined gap in the retarded spectral function. In this regime the weight of the occupied density of states decreases at the lower-edge of the conduction band, but the weight at upper-edge of the conduction band does not change at

all, which is inconsistent with impact ionization. In the inset of Fig. 8(a), we show the total occupation above the Fermi-level as a function of time. After photo-excitation, the integrated spectral weight decreases rapidly with time and reaches saturation at short time scales. We do not observe an increase at later times, which shows that impact ionization processes are not relevant on the timescale of our simulation when the local Coulomb interaction is smaller than ionic potential.

In Fig. 8(b), we consider the case where the ionic potential is comparable to the Coulomb interaction ($U/\Delta = 1.0$). In this case, there is already some spectral weight at the Fermi-level. One can observe that the occupied density of states increases at the lower-band edge of the conduction band and decreases at the upper-band edge decreases, and the overall integrated spectral weight above $\omega = 0$ increases at later times (inset of Fig. 8). Both signatures indicate impact ionization processes take place in this regime. Similarly, we can also identify signatures of impact ionization process when U is greater than the ionic potential as shown in Fig. 8(c).

The precise time-dependent change of the occupied density of states can be used to quantify the significance of impact ionization process at later times in the relaxation process. In Fig. 9, we show the difference of $A^<(t, \omega)$ between large times and some initial time $t = 18$ for $U/\Delta = 1.0$ and $t = 24$ for $U/\Delta = 1.375$. The time-dependent change of the occupied density of states is positive for frequencies below $\omega \sim 0.625$, and negative above 0.625 . The ratio of the increase of the weight below $\omega = 0.625$ to the decrease of weight above $\omega = 0.625$ can therefore give an estimate of number of mobile carriers produced in impact ionization processes. We find that this ratio is roughly 1.4 for $U/\Delta = 1.0$ and 1.25 for $U/\Delta = 1.375$ whereas relaxation only via impact ionization would suggest a ratio of three.³³ This implies that impact ionization processes are less significant in corre-

lated band insulators than in small gap Mott insulators. Probably multi-particle scattering mechanisms are also significant in the rapid thermalization of correlated band insulators.

V. CONCLUSION

In conclusion, we have studied the photo-excitation dynamics of correlated band insulators in the ionic Hubbard model. Depending on the ratio of the interaction U and the ionic potential Δ , we observe a qualitatively different behavior: For $U \lesssim \Delta$, the spectrum itself is weakly influenced by the excitation (apart from a slight photo-induced screening of the gap, which is described by the Hartree shift of the bands.) The relaxation of the system in this regime is characterized by intra-band carrier scattering, leading to a non-thermal intermediate state with separate thermal distributions of electrons and holes. Above a crossover $U \approx \Delta$, the behavior changes. Photo-excitation can lead to a rapid renormalization of the spectrum, a filling-in of the gap, and fast thermalization. This rapid thermalization of a small gap insulator is reminiscent of the thermalization of small gap Mott insulators,³⁰ but in contrast to Mott insulators impact ionization processes³³ are less significant. The strong renormalization of the spectral function indicates that the dynamics of the correlated band insulator in this regime is no longer well described by mere quasi-particle

scattering in rigid bands, which would be captured by kinetic equations.

In equilibrium, two systems with an identical gap in the spectral function can have very different ratios U/Δ . For example, an insulator with $U/\Delta \gtrsim 1$ and a gap Δ_* can be compared to an ideal band insulator with ionic potential Δ_* and $U \ll \Delta_*$. The present analysis shows how these two systems with very similar equilibrium single particle properties can be distinguished by their dynamical behavior. This may be used to classify weakly interacting insulators as either band-insulators or correlated band insulators. In equilibrium, a qualitative distinction of correlated band insulators and band insulators may be based on a different behavior of spin and charge gaps,^{6,7,19} and it will be interesting to see whether these pictures can be linked to the dynamical behavior. We are leaving these questions future work. The observed crossover from a non-thermal state to a thermal state can potentially be found in $\text{SrRu}_{1-x}\text{Ti}_x\text{O}_3$ and some of the 3d transition metal oxides with crystal field splitting.²⁹

ACKNOWLEDGMENTS

We acknowledge fruitful discussions with Yusuf Mohammed, and financial support from the ERC Starting grant No. 716648. The calculations have been done at the PHYSnet cluster of the university of Hamburg.

-
- * nagamalleswararao.d@gmail.com
- ¹ C. Giannetti, M. Capone, D. Fausti, M. Fabrizio, F. Parmigiani, and D. Mihailovic, *Advances in Physics* **65**, 58 (2016).
 - ² D. Fausti, R. I. Tobey, N. Dean, S. Kaiser, A. Dienst, M. C. Hoffmann, S. Pyon, T. Takayama, H. Takagi, and A. Cavalleri, *Science* **331**, 189 (2011).
 - ³ L. Stojchevska, I. Vaskivskyi, T. Mertelj, P. Kusar, D. Svetin, S. Brazovskii, and D. Mihailovic, *Science* **344**, 177 (2014).
 - ⁴ I. Vaskivskyi, J. Gospodaric, S. Brazovskii, D. Svetin, P. Sutar, E. Goreschnik, I. A. Mihailovic, T. Mertelj, and D. Mihailovic, *Science Advances* **1** (2015), 10.1126/sciadv.1500168.
 - ⁵ K. Nasu, “Photoinduced phase transitions,” (World Scientific, Singapore, 2004).
 - ⁶ A. P. Kampf, M. Sekania, G. I. Japaridze, and P. Brune, *Journal of Physics: Condensed Matter* **15**, 5895 (2003).
 - ⁷ G. I. Japaridze, R. Hayn, P. Lombardo, and E. Müller-Hartmann, *Phys. Rev. B* **75**, 245122 (2007).
 - ⁸ S. R. Manmana, V. Meden, R. M. Noack, and K. Schönhammer, *Phys. Rev. B* **70**, 155115 (2004).
 - ⁹ C. D. Batista and A. A. Aligia, *Phys. Rev. Lett.* **92**, 246405 (2004).
 - ¹⁰ A. Garg, H. R. Krishnamurthy, and M. Randeria, *Phys. Rev. Lett.* **97**, 046403 (2006).
 - ¹¹ S. S. Kancharla and E. Dagotto, *Phys. Rev. Lett.* **98**, 016402 (2007).
 - ¹² L. Craco, P. Lombardo, R. Hayn, G. I. Japaridze, and E. Müller-Hartmann, *Phys. Rev. B* **78**, 075121 (2008).
 - ¹³ N. Paris, K. Bouadim, F. Hebert, G. G. Batrouni, and R. T. Scalettar, *Phys. Rev. Lett.* **98**, 046403 (2007).
 - ¹⁴ K. Byczuk, M. Sekania, W. Hofstetter, and A. P. Kampf, *Phys. Rev. B* **79**, 121103 (2009).
 - ¹⁵ A. J. Kim, M. Y. Choi, and G. S. Jeon, *Phys. Rev. B* **89**, 165117 (2014).
 - ¹⁶ A. Hoang, *Journal of Physics: Condensed Matter* **22**, 095602 (2010).
 - ¹⁷ A. Garg, H. R. Krishnamurthy, and M. Randeria, *Phys. Rev. Lett.* **112**, 106406 (2014).
 - ¹⁸ P. Werner and A. J. Millis, *Phys. Rev. Lett.* **99**, 126405 (2007).
 - ¹⁹ M. Sentef, J. Kuneš, P. Werner, and A. P. Kampf, *Phys. Rev. B* **80**, 155116 (2009).
 - ²⁰ A. Euverte, S. Chiesa, R. T. Scalettar, and G. G. Batrouni, *Phys. Rev. B* **87**, 125141 (2013).
 - ²¹ G. Moeller, V. Dobrosavljević, and A. E. Ruckenstein, *Phys. Rev. B* **59**, 6846 (1999).
 - ²² A. Fuhrmann, D. Heilmann, and H. Monien, *Phys. Rev. B* **73**, 245118 (2006).
 - ²³ S. S. Kancharla and S. Okamoto, *Phys. Rev. B* **75**, 193103 (2007).
 - ²⁴ M. Fabrizio, *Phys. Rev. B* **76**, 165110 (2007).
 - ²⁵ H. Hafermann, M. I. Katsnelson, and A. I. Lichtenstein, *EPL (Europhysics Letters)* **85**, 37006 (2009).

- ²⁶ H. Haug and A. P. Jauho, “Quantum kinetics in transport and optics of semiconductors,” (Springer Series in solid-state sciences 123).
- ²⁷ H. Aoki, N. Tsuji, M. Eckstein, M. Kollar, T. Oka, and P. Werner, [Rev. Mod. Phys. **86**, 779 \(2014\)](#).
- ²⁸ M. Eckstein, M. Kollar, and P. Werner, [Phys. Rev. B **81**, 115131 \(2010\)](#).
- ²⁹ K. Maiti, R. S. Singh, and V. R. R. Medicherla, [Phys. Rev. B **76**, 165128 \(2007\)](#).
- ³⁰ M. Eckstein and P. Werner, [Phys. Rev. B **84**, 035122 \(2011\)](#).
- ³¹ J. K. Freericks, H. R. Krishnamurthy, and T. Pruschke, [Phys. Rev. Lett. **102**, 136401 \(2009\)](#).
- ³² D. Golež, L. Boehnke, H. U. R. Strand, M. Eckstein, and P. Werner, [Phys. Rev. Lett. **118**, 246402 \(2017\)](#).
- ³³ P. Werner, K. Held, and M. Eckstein, [Phys. Rev. B **90**, 235102 \(2014\)](#).